DFT rationalization of the room-temperature luminescence properties of Ru(bpy) 3 2+ and Ru(tpy) 2 2+ : 3MLCT–3MC minimum energy path from NEB calculations and emission spectra from VRES calculations

Adrien Soupart, Isabelle M. Dixon, Fabienne Alary, Jean-Louis Heully

Theoretical Chemistry Accounts (**2018**) *137*:37
https://doi.org/10.1007/s00214-018-2216-1

DFT rationalization of the room temperature luminescence properties of $Ru(bpy)_3^{2+}$ and $Ru(tpy)_2^{2+}$: ^{3}MLCT-^{3}MC minimum energy path from NEB calculations and emission spectra from VRES calculations

Adrien Soupart, Isabelle M. Dixon,* Fabienne Alary, Jean-Louis Heully

Laboratoire de Chimie et Physique Quantiques, UMR 5626 CNRS - Université de Toulouse, France.

Corresponding Author : * Isabelle M. Dixon. E-mail address: isabelle.dixon@irsamc.ups-tlse.fr

ORCID ID 0000-0001-5551-6715

Keywords: theoretical photochemistry – energy barriers – photophysics – ruthenium

Abstract

Extensive experimental data covering 40 years of research are available on $Ru(bpy)_3^{2+}$ and $Ru(tpy)_2^{2+}$, which are the archetypes of inorganic photochemistry. The last decade has enabled computational chemists to tackle this topic through density functional theory and to shed some new light on our old friends. For the first time, this theoretical study maps the minimum energy path linking the ^{3}MLCT (metal-to-ligand charge transfer) and the ^{3}MC (metal centred) states with the nudged elastic band (NEB) method, also providing the calculation of the corresponding energy barrier. Remarkably, the obtained data are in very good agreement with the experimental activation energies reported from variable temperature luminescence measurements. Calculation of vibrationally resolved electronic spectra (VRES) is also in excellent agreement with the experimental emission maximum and bandshape of $Ru(bpy)_3^{2+}$. Additionally, the ^{3}MC-GS minimum energy crossing point (MECP) was optimized for each complex. The combination of these data rationalizes the room-temperature luminescence of the bpy complex and non-luminescence of the tpy complex.

Acknowledgements

This article is dedicated to Jean-Pierre Sauvage on the occasion of his 2016 Nobel Prize.
We thank the French Ministry for Higher Education and Research for a Ph. D. fellowship to AS.
This work was performed using HPC resources from CALMIP (Grant 2017-[p1112]).

Introduction

$Ru(bpy)_3^{2+}$, and to a lesser extent $Ru(tpy)_2^{2+}$, are the archetypes of inorganic, or supramolecular, photochemistry. In about 40 years, a wealth of publications have reported their spectroscopic studies and potential applications, and those of their numerous derivatives, in various experimental conditions. Several reviews summarize this data [1],[2],[3],[4],[5]. On the other side, theoretical inorganic photochemistry has significantly matured in the past 10 years. Density functional based methods have particularly enabled computational photochemists to approach photophysical events taking place in Ru(II) polypyridine complexes, such as ground state geometries and Franck-Condon excited state distribution [6],[7],[8],[9],[10],[11], ^{3}MLCT (metal-to-ligand charge transfer) [12],[13],[14],[15],[16] and ^{3}MC (metal centred) [17],[18],[19] excited state relaxation, triplet-triplet internal conversion [20],[21],[22], luminescence [12],[16],[17],[23],[24] or non radiative deactivation [25],[26]. Some of these studies are meant to rationalize experimental observations or unravel complex mechanisms; others serve as predictive tool to anticipate the properties of yet unknown compounds. Ru(II) polypyridine complexes are also used to teach inorganic photophysics in a computational chemistry class [27] or in the field of photoredox catalysis [28]. This study aimed at confronting the emission data on the two cited archetypes (emission wavelength and bandshape, energy barriers) and the conclusions drawn from modern computational tools that are available in an open theoretical chemistry package (Orca) [29] in order to rationalize the room-temperature luminescence of $Ru(bpy)_3^{2+}$ vs non-luminescence of $Ru(tpy)_2^{2+}$. On the basis of previously described ^{3}MLCT and ^{3}MC states [17] [18] [19] [20] [21] [22] [25] [30], which were reoptimized, we here report for the first time the computation of the ^{3}MLCT-^{3}MC minimum energy path for $Ru(bpy)_3^{2+}$ and $Ru(tpy)_2^{2+}$, using the nudged elastic band method, a method that is popular in solid state physics and surface science for ground state potential energy surface exploration [31],[32] but has been reported scarcely in molecular inorganic photochemistry [33],[34], to the best of our knowledge. Very recently we have reported the successful use of this method in the context of deciphering photoreactivity mechanisms [35].

Summary of experimental luminescence data

In Ru(II) polypyridine complexes, the cascade of photoinduced elementary events, as well as their timescales, are now well established : following light absorption into a ^{1}MLCT state, ultrafast and quantitative intersystem crossing occurs to populate a vibrationally hot ^{3}MLCT manifold (<300 fs) [36], followed by internal conversion to the lowest ^{3}MLCT state and vibrational cooling to the thermally equilibrated (THEXI) [37] ^{3}MLCT state (10-20 ps) [38],[39]. Fluorescence of the ^{1}MLCT state of $Ru(bpy)_3^{2+}$ has also been observed on very short timescales [40]. In $Ru(bpy)_3^{2+}$, the (de)localization of the unpaired electron on the ligand(s) has been the subject of specific spectroscopic studies, concluding that (i) the initially formed D3-symmetric MLCT state evolved into a C2-symmetric MLCT state bearing an unpaired electron localized on a single bpy ligand, and (ii) this charge localization process is coupled to solvation dynamics and occurs within 60 fs in acetonitrile at room temperature [41]. This lowest ^{3}MLCT state can then either deactivate radiatively (i.e. by phosphorescence) or nonradiatively, or the system undergoes internal conversion to a ^{3}MC state. For $Ru(tpy)_2^{2+}$, from UV-visible transient absorption spectroscopy, the lifetime of the ^{3}MLCT state is τ=124 ps [42]. ^{3}MLCT-^{3}MC equilibration has been reported with a 2.3 ps timecale [42], on the basis of a loss in the reduced ligand near-UV absorption band without concomitant recovery of the ground-state bleach. From the ^{3}MC state, the GS can be repopulated by nonradiative deactivation, with a 18 ps timescale [42]. The ^{3}MLCT luminescence quenching is mainly ascribed to a thermally accessible ^{3}MC state, which is non emissive [43].

In acetonitrile solution, room temperature emission studies describe $Ru(tpy)_2^{2+}$ as essentially non luminescent ($\tau < 0.005$ µs) [3], while $Ru(bpy)_3^{2+}$ emits at λ=615 nm (τ=1.1 µs) [44]. From variable

temperature time resolved emission measurements, the activation energy required to populate the ^{3}MC state from the ^{3}MLCT state was estimated to be 1700 cm^{-1} (5 kcal/mol) for $Ru(tpy)_2^{2+}$ in BuCN [45]. The corresponding activation energy for $Ru(bpy)_3^{2+}$ was estimated to be 3800 cm^{-1} (11 kcal/mol) in MeCN [46]. In terms of emission properties, the difference between $Ru(bpy)_3^{2+}$ and $Ru(tpy)_2^{2+}$ is explained essentially on a structural basis : two terpyridine ligands provide a weaker ligand field to the metal, due to their unfavorable bite angle (157°). This weaker ligand field stabilizes the ^{3}MC (ligand-field) state, thus allowing efficient non radiative deactivation of the ^{3}MLCT state.

The structural parameters of excited states are experimentally accessible through the use of time resolved X-ray absorption spectroscopy (EXAFS and XANES), thanks to the recent developments of ultrafast synchrotron beams [47]. This type of technique allows to probe the metal's coordination sphere (symmetry, coordination number, nature of bound atoms, average M-L distances), oxidation and spin state [48],[49],[50]. It is worth noting that the only available data for Ru complexes concern the ^{3}MLCT state of $Ru(bpy)_3^{2+}$ [51],[52],[53]. To our knowledge, no structural data is available on ^{3}MC states of Ru(II) complexes.

Computational details

Geometry optimizations were performed without symmetry with Orca 3.0 [29] using the B3LYP functional [54],[55], a relativistic small core pseudopotential on Ru (SD28) [56], the def2-TZVP basis set [57], and the empirical D3 dispersion correction [58],[59] (such conditions apply throughout). The restricted Kohn-Sham formalism was used for ground states, while its unrestricted analogue was used for triplet states. SCF convergence was achieved using the DIIS algorithm followed by a semi-quadratic SOSCF converger. Two complete sets of geometries were obtained : gas phase geometries, which are in excellent agreement with X-ray data [60],[61], and geometries in MeCN solvent, as modelled by SMD [62], which were optimized starting from the gas phase ones. Frequency calculations were run at the same level of theory and the absence of imaginary frequencies ascertained the nature of these points as minima. Molecular orbitals were viewed using Gabedit [63]. Mulliken spin densities on Ru were used as a straightforward descriptor of the electronic nature of the triplet excited state (~0.9 for a ^{3}MLCT state, ~1.8 for a ^{3}MC state). Orbital analysis was systematically undertaken to view the localization of the unpaired electrons.

^{3}MC/GS minimum energy crossing points (MECPs) were optimized using Orca 3.0 using the same conditions, starting from a ^{3}MC-type geometry. Frequency calculations were also run on the MECP geometries (SurfCrossNumFreq keyword), in gas phase and in solvent.

VRES (vibrationally resolved electronic spectra) calculations (IMDHOT model with T=298 K or 77 K, setting the line-broadening factor to $\Sigma = 500\ cm^{-1}$ in order to obtain the same full width at half maximum as in the experimental spectra of refs [46] and [64], i.e. FWHM = 2870 cm^{-1}) were performed to model emission spectra (data computed at 298 K shown in Figure 1 for $Ru(bpy)_3^{2+}$ and Figure S1 for $Ru(tpy)_2^{2+}$). Such calculations require the energy gap between the relevant states and the hessian for the ground state (in solvent), first using the orca_vib module to compute the dimensionless shifts between ground and excited state geometries, and then using the orca_asa program [65],[66] to incorporate the effect of the ground state vibrational frequencies. The IMDHOT model implemented in orca_asa is based on the following approximations, which are physically meaningful and computationally extremely efficient: the ground and excited potential energy surfaces are assumed to be harmonic; the vibrations of the excited state are assumed to be the same as those of the ground state [67]; the minimum of the excited PES is simply shifted with respect to the minimum of the ground state PES (dimensionless displacements along all normal modes).

The ^{3}MLCT-^{3}MC minimum energy paths were optimized with the nudged elastic band (NEB) method [31],[32] using a python module developed in the Clancy group [68] that is interfaced with Orca 3.0. The convergence criterion was set to 0.03 eV/Å. A 10-frame initial path was prepared by interpolating start and end geometries using the IDPP method [69]. IDPP initial paths are given in Supporting Information. The geometries were previously processed using lab-developed programs to minimize the discrepancy between start and end geometries. These calculations were performed using the BFGS algorithm at the same level of theory as all the geometry optimizations (minima and MECPs). Two sets of calculations were performed : gas phase NEB calculation between gas phase minima (shown in Figure S2), and SMD NEB calculation between SMD minima (shown in Figure 2 and converged paths given in Supporting Information). Not surprisingly, comparing the results from the two sets of data (gas phase and SMD) and confronting them to experimental values confirms that the highest level of methodology is desirable when strong comparison to experiment is wanted.

Results and discussion

* General considerations

Charge transfer states, being intrisically stabilized in polar medium, are particularly sensitive to solvent [70]. Their electronic structure, in terms of localization of the transferred electron, can also be directly solvent-dependent. Solvent effects are more limited on GS and ^{3}MC states, which bear much smaller dipole moments [71]. Such effects can be taken into account using different approaches. The most common, and least computationally demanding, approach in static DFT calculations considers the solvent as a polarized continuum which may accept some leaking electron density (e.g. COSMO) [72]. This approach has in particular been widely used for the calculation of absorption spectra. The SMD model [62] goes beyond COSMO since it includes the cavitation energy, i.e. the energetic cost due to tear apart solvent molecules in order to host the solute. The B3LYP hybrid functional has been shown to perform very well in reproducing ground state and ^{3}MLCT geometries of many ruthenium(II) polypyridine complexes (experimental structural data on their ^{3}MC states, e.g. from picosecond X-ray absorption spectroscopy, are still awaited), as well as their absorption and emission energies and spectral profiles, which involve MLCT states. Therefore this functional was used throughout this work.

* Emission spectra

ΔSCF calculations (in the case of Ru complexes, single point energy calculation of the ground state species at the ^{3}MLCT geometry) give a rough estimate of the emission wavelength of a luminophore. Some approximations are due to the fact that (i) the ^{3}MLCT zero-point energy is neglected, (ii) vibrational levels are neglected, (iii) the anharmonicity of the potential energy surfaces is neglected, and (iv) environment effects are generally either neglected (counterions) or modelled (solvent). This calculation yielded emission wavelengths of 689 nm (1.80 eV) for $Ru(bpy)_3^{2+}$ (blue bar on Figure 1) and 697 nm (1.78 eV) for $Ru(tpy)_2^{2+}$ in MeCN (Table 1).

Following the Franck-Condon principle, approaches that take into account the Boltzmann population of the ^{3}MLCT state and the vibrational levels of the ground state include the contributions from the 0-0, 0-1, 0-2, …, 0-n, 1-0, … transitions, at a given temperature. As shown on Figure 1 for $Ru(bpy)_3^{2+}$, such vibrationally resolved electronic spectra (VRES) model much more accurately experimental emission bandshapes [16]. Therefore, computationally efficient procedures such as the one implemented in Orca should systematically be used to model emission spectra. Such VRES calculations emission spectra in MeCN yielded an emission maximum at 626 nm (1.98 eV) for $Ru(bpy)_3^{2+}$ (Figure 1), in very good

agreement with the experimental value of 620 nm [46], and at 663 nm for $Ru(tpy)_2^{2+}$ (1.87 eV, Figure S1). Obtaining a correct band maximum is necessary, but not sufficient. As shown on Figure 1 for the room temperature emission of $Ru(bpy)_3^{2+}$, the bandshape of the experimental emission spectrum (particularly its asymmetry) [64] is also very well reproduced using the VRES method.

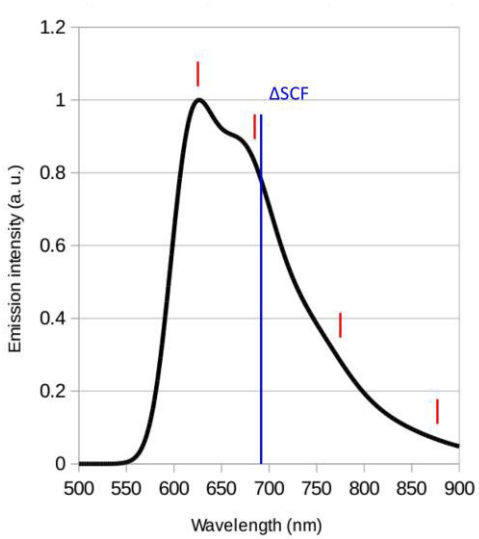

Fig. 1 Computed emission spectra for $Ru(bpy)_3^{2+}$ (298 K, B3LYP, SMD-MeCN). The blue line shows the position of the emission maximum according to a ΔSCF calculation. The black spectrum was computed using the VRES method. The red bars represent the vibrational spacing of 1515 cm^{-1}.

Another interesting feature of the VRES method is that the vibrational spacing enables us to identify the localization of the excitation (Figure 1). In Ru(II) polypyridine complexes, the vibration that is mostly responsible for the vibronic structure is a C–C stretch at 1515 cm^{-1}, in agreement with the 1500 cm^{-1} experimental value measured from time-resolved resonance Raman spectroscopy and identified as signature of the bpy radical anion [39],[67],[73]. This corresponds to the stretching of the interpyridine bond of the reduced bpy ligand, which is consecutive to the population of a π* orbital that is bonding between these two carbon atoms. As a consequence of the population of this orbital, the interpyridine distance is reduced from 1.468 (GS) to 1.412 Å (^{3}MLCT state) (values in solvent) (the Ru–N distances to the reduced bpy also decrease from 2.074 to 2.046 Å, for electrostatic reasons, see Chart 1).

Table 1: Computed and experimental [3] emission wavelength maxima (nm). Emission energies in eV are given in parentheses.

	exp 298 K	theo ΔSCF	theo VRES 298 K	exp 77 K	theo VRES 77 K	theo ΔSCF'
$Ru(bpy)_3^{2+}$	620[a] (2.00)	689 (1.80)	626[b] (1.98)	580[c] (2.14)	624[b] (1.99)	566 (2.19)
$Ru(tpy)_2^{2+}$	---	697	663[b]	602[d]	660[b]	626

(1.78) (1.87) (2.06) (1.88) (1.98)

[a] in MeCN; [b] in MeCN (SMD); [c] in MeOH/EtOH; [d] in BuCN.

Applying the same methodology to model 77 K spectra of MLCT emitting states, which are very sensitive to solvent, necessarily yields bathochromically shifted emission energies. This is due to the fact that in the VRES calculation the energy gap is estimated between the ^{3}MLCT and GS geometries, both relaxed in solvent (in their own solvation environment), whereas in the low temperature experiment (below the fluid-to-glass transition) the environment is frozen around the GS geometry. This underlines the so-called rigidochromic effect [74]. Solvation dynamics being precluded in frozen matrix, the ^{3}MLCT state is actually less stabilised in the experiment (where it is surrounded by the GS solvation cage) [71] than in the calculation. Therefore the calculated emission energy is underestimated. The shift of the calculated 77 K ^{3}MLCT emission energy can be estimated by performing two gas phase single point energy calculations, at the ^{3}MLCT geometry optimised in solvent, for a singlet and a triplet state. This gives a ΔSCF' value that can be compared to the one given by the VRES calculation : it turns out that ΔSCF' = E(theo-VRES-77 K) + 0.2 eV for $Ru(bpy)_3^{2+}$ and ΔSCF' = E(theo-VRES-77 K) + 0.1 eV for $Ru(tpy)_2^{2+}$. The same shifts are found between gas phase and solvent ^{3}MLCT-GS gaps (Table 2), and between the room temperature ΔSCF and VRES emission energies (Table 1). The blue shift is larger for $Ru(bpy)_3^{2+}$ because its ^{3}MLCT state has a larger dipole moment (10 D, vs. 7 D for the ^{3}MLCT state of $Ru(tpy)_2^{2+}$), which makes it more sensitive to solvent effects.

* Minima on the singlet and lowest triplet PES

In the case of Ru(II) polypyridine complexes, optimizing ground state geometries is obviously a standard procedure. The inclusion of classical dispersion forces [58],[59] greatly improves the computed bond lengths and yields an excellent agreement with crystallographic interatomic distances [60],[61]. The real challenge lies in the capacity to optimize several different triplet states, since DFT is a variational method minimizing the energy of any state of given spin multiplicity. In addition, convergence of the wavefunction on open-shell systems is nontrivial, and convergence on the desired electronic excited state can be really challenging, even more so when the density of states is high.

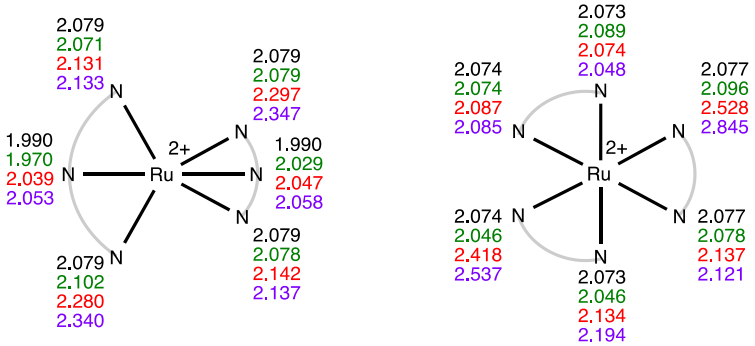

Chart 1. Ru-N distances in the ground state (black), ^{3}MLCT (green), ^{3}MC (red) and ^{3}MC/GS MECP (purple) geometries for $Ru(tpy)_2^{2+}$ (left) and $Ru(bpy)_3^{2+}$ (right), in solvent (B3LYP-D3 + SMD-MeCN).

Computed ^{3}MLCT geometries [17],[23] are easily obtained starting the optimization from the ground state equilibrium geometries, and match the available structural data (the average Ru–N distance

decreases) [51],[52],[53]. Ground state and ^{3}MLCT equilibrium geometries are similar in many respects (Chart 1). In terms of electronic structure, for $Ru(bpy)_3^{2+}$, the lowest ^{3}MLCT state is of C2 symmetry in solvent (electron localized on one ligand), while it is of D3 symmetry in vacuum (electron delocalized over the three ligands) [16],[17]. The ^{3}MLCT state of $Ru(tpy)_2^{2+}$ has the same electronic structure whether in the gas phase or in solvent, with the electron being transferred to one tpy ligand in both cases. Additionally, the GS-^{3}MLCT energy gap (Table 2) is significantly reduced from the gas phase to solvent, since the ^{3}MLCT state is more stabilised than GS by solvation [71], which will directly affect the photophysics of the complexes.

On the other hand, the first full and unambiguous description of a ^{3}MC DFT-optimized geometry [17] was obtained after providing a starting geometry displaying major bond elongations with respect to the ground state geometry, namely two trans elongated Ru-N bonds for $Ru(bpy)_3^{2+}$. This successful optimization has allowed us to quantify the extent of structural distortions that are involved in the ^{3}MC state of $Ru(bpy)_3^{2+}$. More recently, the excited ^{3}PES of $Ru(tpy)_2^{2+}$ has also been thoroughly examined by DFT and TDDFT [18],[20],[21],[22]. The general features of these ^{3}MC states are significant (up to 0.4 Å, Chart 1) Ru-N elongation along two or four directions, depending on whether a pseudo d_{z2} or pseudo d_{x2-y2} antibonding dσ* orbital is populated.

^{3}MLCT and ^{3}MC states were reoptimized here to work with a fully consistent set of states and at the same level of theory. The energy gaps between minima (ΔE) are given in Table 2 (similar trends are observed for ΔE, Δ(E+ZPE) or ΔG (298 K) energy gaps, see Table S3). As expected, the optimized ^{3}MLCT state is stabilized in solvent, which decreases the ^{3}MLCT-GS gap and increases the ^{3}MLCT-^{3}MC gap. In solvent, the ^{3}MLCT-^{3}MC energy gap is larger for $Ru(bpy)_3^{2+}$ (0.18 eV, 4 kcal/mol) than for $Ru(tpy)_2^{2+}$ (0.13 eV, 3 kcal/mol), but not much larger (and is similar within the accuracy of our method). It is thus required to go beyond this simple picture to rationalize the luminescence of one vs. the non-luminescence of the other.

Table 2. Energy gaps and energy barriers (eV) for $Ru(bpy)_3^{2+}$ and $Ru(tpy)_2^{2+}$, in the gas phase and in solvent (B3LYP-D3 ± SMD-MeCN). Values in kcal/mol in parentheses.

	$Ru(bpy)_3^{2+}$		$Ru(tpy)_2^{2+}$	
	gas phase	solvent	gas phase	solvent
^{3}MLCT-GS gap	2.22[a] (51.2)	2.03[b] (46.8)	2.10 (48.4)	2.00 (46.1)
^{3}MC-GS gap	2.16 (49.8)	2.21 (51.0)	2.11 (48.7)	2.13 (49.1)
^{3}MLCT-^{3}MC gap	0.06 (1.4)	–0.18 (–4.2)	–0.01 (–0.3)	–0.13 (–3.0)
^{3}MLCT → ^{3}MC barrier	0.20 (4.7)	0.38 (8.7)	0.09 (2.0)	0.18 (4.1)
^{3}MC → ^{3}MLCT barrier	0.26 (6.1)	0.20 (4.6)	0.07 (1.6)	0.06 (1.3)
$^{3/1}$MECP-^{3}MC gap	0.28 (6.5)	0.27 (6.2)	0.04 (0.9)	0.04 (0.9)

[a] The gas-phase ^{3}MLCT geometry has D3 symmetry. [b] The lowest ^{3}MLCT geometry in solvent has C2 symmetry.

***** Exploring the ^{3}MLCT-^{3}MC internal conversion process

The ^{3}MLCT-^{3}MC minimum energy path (MEP) can be explored theoretically by two means : (i) using the strings method [75],[76] or the nudged elastic band method [31],[32], which minimize the energy path connecting the two minima using energies and gradients, thus allowing to quantify the activation barrier ; (ii) undertaking a transition state (TS) search followed by intrinsic reaction coordinate calculations to connect the TS with the two minima [77]. Both methods estimate the activation barrier $\Delta E^{\neq}$, which is the most relevant data for comparison with experiment, but none have been reported so far for $Ru(bpy)_3^{2+}$ and only method (ii) has been reported for $Ru(tpy)_2^{2+}$ [22]. Alternatively, the topology of the triplet PES was probed by running (computationally demanding) TDDFT 2D PES scans [20],[21]. We have previously compared methods (i) and (ii) on another Ru(II) complex and have shown that they gave comparable results [34]. The two MEPs calculated using method (i) in MeCN (SMD) are shown on Figure 2 (MEPs in gas phase are shown on Figure S2 and are the direct consequence of relative MLCT destabilization in gas phase). The evolution of the Mulliken spin population on ruthenium can be followed along the MEP. This shows that the ^{3}MLCT character is preserved for about half the way, after which electron density is suddenly transferred back to the metal to form a ^{3}MC state (Tables S1-S2).

In the case of $Ru(bpy)_3^{2+}$, the profile of the MEP is relatively abrupt towards the ^{3}MC state (which is a true minimum). This profile was qualitatively confirmed by two additional calculations:

- a single point energy calculation at a geometry corresponding to x=1.1 (obtained by linear extrapolation along the MEP coordinate) indicated that this structure had an energy more than 1 kcal/mol higher than that of the ^{3}MC minimum.
- another NEB calculation was run starting from a 20-image IDPP path. This yielded a slightly smoother but very similar energy profile.

Therefore the ^{3}MLCT → ^{3}MC minimum energy path appears to be genuinely relatively abrupt towards the ^{3}MC minimum.

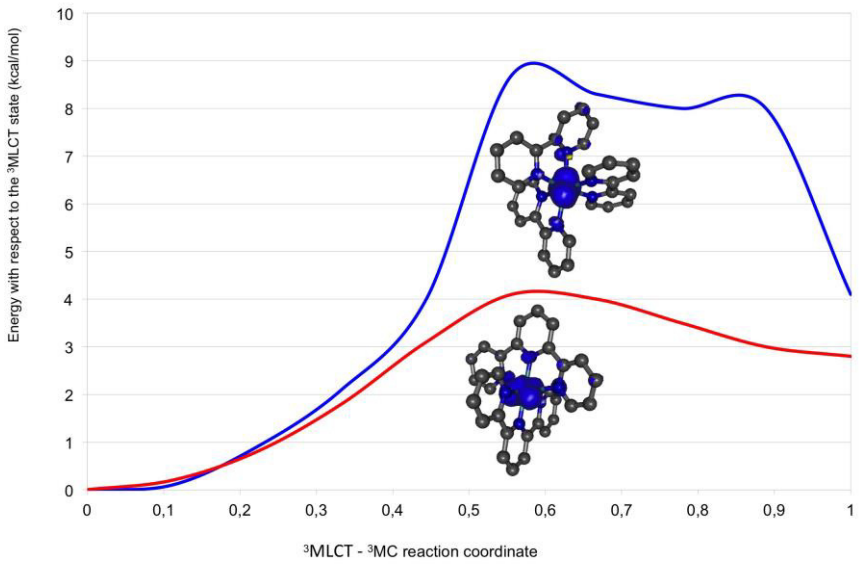

Fig. 2 Computed NEB minimum energy path along the ^{3}MLCT → ^{3}MC reaction coordinate for $Ru(bpy)_3^{2+}$ (blue line) and $Ru(tpy)_2^{2+}$ (red line) (B3LYP-D3, SMD-MeCN). The ^{3}MLCT state is found at x=0 and the ^{3}MC state at x=1. x is a reaction coordinate that corresponds to the geometrical advancement measuring the percentage of geometric distortion between start and end geometries. Plots of the Mulliken spin densities at the optimized transition states

The activation barriers computed using the NEB method are 4.1 kcal/mol (0.18 eV) for $Ru(tpy)_2^{2+}$ in MeCN (2.0 kcal/mol = 0.09 eV in the gas phase), and 8.7 kcal/mol (0.38 eV) for $Ru(bpy)_3^{2+}$ in MeCN (4.7 kcal/mol = 0.20 eV in the gas phase). Both values compare very well with the experimental values (activation energies derived from variable temperature time resolved emission measurements : 5 kcal/mol [45] for $Ru(tpy)_2^{2+}$ and 11 kcal/mol [46] for $Ru(bpy)_3^{2+}$). The stabilization of the ^{3}MLCT state in solvent doubles the MLCT → MC energy barrier with respect to the gas phase calculation. The ^{3}MLCT-^{3}MC energy barrier is significant for $Ru(bpy)_3^{2+}$ in solvent, which is consistent with its luminescence properties and with ultrafast time-resolved spectroscopic studies (transient absorption [78] and IR [79],[30]), which indicate that no intermediate state is populated during the decay of the ^{3}MLCT state of $Ru(bpy)_3^{2+}$. On the other hand, the ^{3}MLCT-^{3}MC energy barrier is small for $Ru(tpy)_2^{2+}$, which is consistent with a non luminescent complex and with excited-state equilibration, as measured by ultrafast transient absorption spectroscopy [42]. The fact that the excited state population of $Ru(tpy)_2^{2+}$ was experimentally found to reside mostly in the ^{3}MLCT state [42] is in perfect agreement with our computed ^{3}MLCT-^{3}MC energy gap and with the forward and reverse energy barriers shown in Table 2. The ^{3}MLCT-^{3}MC energy barrier computed using the NEB method also fully agrees with previous computational data obtained at a slightly different level of theory by Persson et al., who estimated this barrier to be 2 kcal/mol in MeCN by TDDFT 2D-PES scans [21], and by Heinze et al. who optimized the ^{3}MLCT-^{3}MC transition state and located it 2 kcal/mol above the ^{3}MLCT minimum in MeCN [22]. Comparing the ^{3}MLCT-^{3}MC energy gaps was insufficient to distinguish the phosphorescence of $Ru(bpy)_3^{2+}$ from the luminescence quenching in $Ru(tpy)_2^{2+}$. The knowledge of the ^{3}MLCT → ^{3}MC energy barrier appears to be crucial to rationalize the observed photophysical properties. In other words, the ^{3}MLCT → ^{3}MC internal conversion process is kinetically driven, rather than thermally driven.

The quality of the NEB MEP was confirmed by transition state optimization in SMD-MeCN starting from NEB crest geometries, which converged on structures of similar energy and geometry as the NEB crests (Tables S5, S7). The Mulliken spin density on Ru at the TS is 1.33 for tpy and 1.61 for bpy, and the MC character at the transition states is also illustrated in plots of their spin densities (Figure 2).

* Evolution from the ^{3}MC state : the ^{3}MC/GS minimum energy crossing point (MECP)

Once the ^{3}MC state is populated, which is favorable for $Ru(tpy)_2^{2+}$ as it involves a low 4 kcal/mol energy barrier, the system may return to the ^{3}MLCT state (^{3}MC → ^{3}MLCT energy barrier) or may decay nonradiatively by crossing the ground state surface (MECP-^{3}MC energy gap). Whether in the gas phase or in solvent, both barriers are of the same order of magnitude for both complexes (Table 2). From a general viewpoint, the relevance of spin crossing phenomena in organometallic reactivity is now well established, and is not limited to first-row transition metals [80],[81],[82]. Photochemical reactions involving coordination compounds are also commonly nonadiabatic, and intersystem crossing is encountered at several stages after photoexcitation (e.g. ^{1}MLCT → ^{3}MLCT or ^{3}MC → GS) [83]. Singlet and triplet potential energy surfaces may particularly cross in regions where the ground state species is largely destabilized by geometric distortions. Along the crossing line lies a point of minimum energy, whose geometry can be optimized using specific algorithms [84],[85],[86],[87]. The position of this MECP, in terms of energy and structure, is particularly important in the framework of inorganic photophysics, when one wants to estimate the ease of nonradiative ground state recovery by ^{3}MC/GS crossing, which is directly related to luminescence quenching. This type of calculation is far from systematic in the literature but is nonetheless essential for the understanding of the photoinduced processes. As pointed before [22], distortions in the ^{3}MC/GS MECP emphasize the distortions in the corresponding ^{3}MC state. This effect is more pronounced for $Ru(bpy)_3^{2+}$, whose two longest bonds are significantly elongated in the MECP (+0.1 to +0.3 Å) than for $Ru(tpy)_2^{2+}$, whose two longest bonds are only moderately elongated in the MECP (+0.05 Å). No major angular variations are noted between

these ^{3}MC states and MECPs. It is noteworthy that the MECP is almost degenerate with the ^{3}MC state in the case of $Ru(tpy)_2^{2+}$, while the MECP-^{3}MC gap is significant in $Ru(bpy)_3^{2+}$ (Table 2). This indicates that the ^{3}MC state can decay nonradiatively more efficiently for the bis(tridentate) complex, in line with the absence of room temperature luminescence. To illustrate the theoretical rationalization of the luminescence properties of $Ru(bpy)_3^{2+}$ and $Ru(tpy)_2^{2+}$, energy gaps and barriers are summarized on Figure 3.

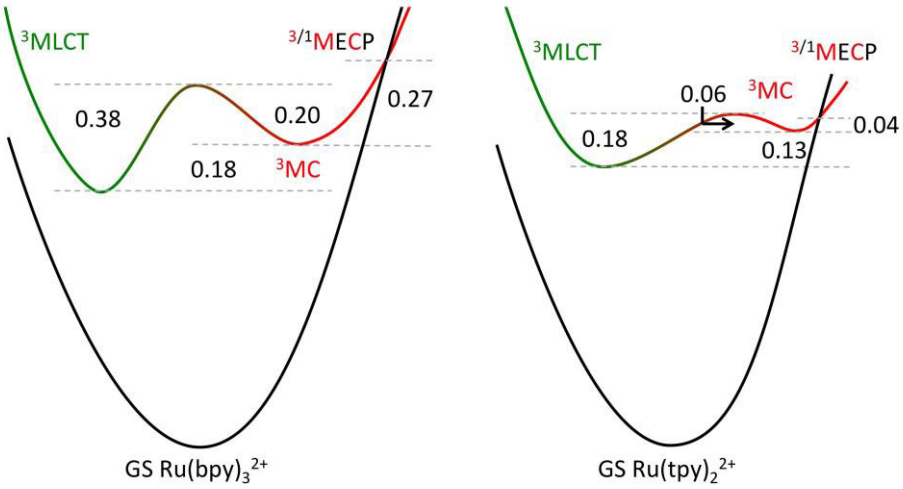

Fig. 3 Schematic potential energy curves with energy gaps in eV, computed in SMD-MeCN

* Investigation of other possible deactivation pathways : direct ^{3}MLCT/GS MECP

Following Heinze's identification of a ^{3}MLCT/GS MECP in cyclometallated bis(tridentate) Ru(II) complexes [88], we were interested to search for such a crossing point, which would be located on the left-hand side of Figure 3. For $Ru(tpy)_2^{2+}$, (i) an MECP optimization starting from the GS geometry converges on the previously found ^{3}MC/GS MECP; (ii) the same is obtained starting from the ^{3}MLCT geometry; (iii) assuming that the distortions in the MECP emphasize the distortions in the corresponding triplet state (as for the ^{3}MC/GS MECP) [25],[88], we built a guess geometry by tilting the central cycle of the tridentate ligand receiving the electron. The dihedral angle between the central and peripheral cycles is about 10° in the ^{3}MLCT geometry and was increased to 30° in the guess geometry, as observed in Heinze's ^{3}MLCT/GS MECP [88]. An MECP optimization starting from this 30°-tilted guess geometry converged on the previously found ^{3}MC/GS MECP. In all three cases, the MECP optimization algorithm thus converges on the ^{3}MC/GS MECP.

To further probe the ^{3}MLCT/GS MECP region, we checked if the preceding angular distortion actually decreases the singlet-triplet gap. To do so, three geometries were interpolated between the ^{3}MLCT and the 30°-tilted geometry and five ΔSCF calculations were performed. The ΔSCF value actually decreases along this distortion coordinate (ΔSCF = 1.68, 1.57, 1.45, 1.35 and 1.27 eV for a tilting angle of 12, 17, 21, 26 and 30°), but insufficiently to approach the crossing seam. Therefore there is no accessible ^{3}MLCT/GS MECP for $Ru(tpy)_2^{2+}$ that could account for an efficient direct nonradiative deactivation channel of the ^{3}MLCT state, in line with the energy gap law and with the fact that the ^{3}MLCT state is only weakly coupled to the ground state [89], whereas the ^{3}MC state is in the strong coupling limit [89],[90]. Similarly, all attempts to optimize a ^{3}MLCT/GS MECP for $Ru(bpy)_3^{2+}$ converged on MC-type MECPs. Having no highly accessible non radiative deactivation pathways (neither through ^{3}MC nor through ^{3}MLCT/GS MECP), $Ru(bpy)_3^{2+}$ is inevitably phosphorescent at room temperature. In the case

of $Ru(tpy)_2^{2+}$, the observed luminescence quenching necessarily involves ^{3}MLCT → ^{3}MC internal conversion, followed by ^{3}MC → GS intersystem crossing through a very accessible ^{3}MC/GS MECP.

Conclusion

State-of-the art DFT calculations not only provide geometries and electronic structures, or enable us to model absorption and emission spectra. They also go well beyond a Jablonski diagram, providing us with energy barriers, minimum energy paths and minimum energy crossing points, which are required to unravel complex multistep mechanisms in the excited state or to rationalize photophysical or photochemical data. This computational study reports, for the first time using the nudged elastic band method, the calculation of the minimum energy paths between the ^{3}MLCT and ^{3}MC minima for $Ru(bpy)_3^{2+}$ and $Ru(tpy)_2^{2+}$, providing us with a computational estimate of the ^{3}MLCT-^{3}MC energy barriers for both complexes, in the gas phase and in solvent, without requiring TS optimization or scanning arbitrary coordinates. In both cases, the data computed in solvent is in very good agreement with the experimental data, both in terms of absolute values and relative values (the barrier being twice larger for the tris(bidentate) complex). The quantitative character of the method is remarkable for such small energy barriers and holds great promise for the future of modern theoretical inorganic photochemistry.

Supporting Information

Gas phase bond lengths; VRES for $Ru(tpy)_2^{2+}$; gas phase NEB calculations; Mulliken spin density along the MEPs; schematic potential energy curves computed in the gas phase; comparison between ΔE / $\Delta(E+ZPE)$ / ΔG (298 K); cartesian coordinates for both complexes (GS, ^{3}MLCT, ^{3}MC and MECP), in the gas phase and in solvent; cartesian coordinates for the ^{3}MLCT-^{3}MC transition states optimized in SMD-MeCN (PDF). IDPP initial paths and converged minimum energy paths (xyz files).

Conflict of Interest: The authors declare that they have no conflict of interest.

References

1. Kalyanasundaram K (1982) Photophysics, Photochemistry and Solar Energy Conversion with tris(bipyridyl)ruthenium(II) and its Analogues. Coord Chem Rev 46:159–244

2. Meyer TJ (1986) Photochemistry of Metal Coordination Complexes: Metal to Ligand Charge Transfer Excited States. Pure Appl Chem 58:1193–1206

3. Juris A, Balzani V, Barigelletti F, et al (1988) Ru(II) Polypyridine Complexes : Photophysics, Photochemistry, Electrochemistry, and Chemiluminescence. Coord Chem Rev 84:85–277

4. Campagna S, Puntoriero F, Nastasi F, et al (2007) Photochemistry and Photophysics of Coordination Compounds: Ruthenium. In: Balzani V, Campagna S (eds) Photochemistry and Photophysics of Coordination Compounds I. Springer, Berlin, Heidelberg

5. Thompson DW, Ito A, Meyer TJ (2013) $[Ru(bpy)_3]^{2+}$* and Other Remarkable Metal-to-Ligand Charge Transfer (MLCT) Excited States. Pure Appl Chem 85:1257–1305 . doi: 10.1351/PAC-CON-13-

6. Daul C, Baerends EJ, Vernooijs P (1994) A Density Functional Study of the MLCT States of $[Ru(bpy)_3]^{2+}$ in D_3 symmetry. Inorg Chem 33:3538–3543

7. Buchs M, Daul C (1998) Geometry Optimization and Excited States of Tris(2,2'-bipyridine)ruthenium(II) Using Density Functional Theory. Chimia 52:163–166

8. Zheng K, Wang J, Shen Y, et al (2001) Electronic Structures and Related Properties of Complexes $M(bpy)_3^{n+}$ (M=Re, Os, and Ir; n=1, 2, and 3, Respectively). J Phys Chem A 105:7248–7253

9. Zheng KC, Wang JP, Peng WL, et al (2002) Theoretical Studies on the Electronic Structures and Related Properties of $[Ru(L)_3]^{2+}$ (L=bpy, bpm, pbz) with DFT Method. J Mol Struct THEOCHEM 582:1–9

10. Stoyanov SR, Villegas JM, Rillema DP (2002) Density Functional Theory Calculations of Selected Ru(II) Two Ring Diimine Complex Dications. Inorg Chem 41:2941–2945 . doi: 10.1021/ic0110629

11. Muhavini Wawire C, Jouvenot D, Loiseau F, et al (2014) Density-Functional Study of Luminescence in Polypyridine Ruthenium Complexes. J Photochem Photobiol Chem 276:8–15 . doi: 10.1016/j.jphotochem.2013.10.018

12. Xie Z-Z, Fang W-H (2005) Electrophosphorescent Divalent Osmium and Ruthenium Complexes: A Density Functional Theory Investigation of their Electronic and Spectroscopic Properties. J Mol Struct THEOCHEM 717:179–187 . doi: 10.1016/j.theochem.2004.11.030

13. Moret M-E, Tavernelli I, Rothlisberger U (2009) Combined QM/MM and Classical Molecular Dynamics Study of $[Ru(bpy)_3]^{2+}$ in Water. J Phys Chem B 113:7737–7744 . doi: 10.1021/jp900147r

14. Moret M-E, Tavernelli I, Chergui M, Rothlisberger U (2010) Electron Localization Dynamics in the Triplet Excited State of $[Ru(bpy)_3]^{2+}$ in Aqueous Solution. Chem - Eur J 16:5889–5894 . doi: 10.1002/chem.201000184

15. Tavernelli I, Curchod BFE, Rothlisberger U (2011) Nonadiabatic Molecular Dynamics with Solvent Effects: A LR-TDDFT QM/MM Study of Ruthenium(II) tris(bipyridine) in Water. Chem Phys 391:101–109 . doi: 10.1016/j.chemphys.2011.03.021

16. Nozaki K, Takamori K, Nakatsugawa Y, Ohno T (2006) Theoretical Studies of Phosphorescence Spectra of Tris(2,2'-bipyridine) Transition Metal Compounds. Inorg Chem 45:6161–6178 . doi: 10.1021/ic052068r

17. Alary F, Heully J-L, Bijeire L, Vicendo P (2007) Is the ^{3}MLCT the Only Photoreactive State of Polypyridyl Complexes? Inorg Chem 46:3154–3165 . doi: 10.1021/ic062193i

18. Borg OA, Godinho SSMC, Lundqvist MJ, et al (2008) Computational Study of the Lowest Triplet State of Ruthenium Polypyridyl Complexes Used in Artificial Photosynthesis. J Phys Chem A 112:4470–4476 . doi: 10.1021/jp8000702

19. Jakubikova E, Chen W, Dattelbaum DM, et al (2009) Electronic Structure and Spectroscopy of $[Ru(tpy)_2]^{2+}$, $[Ru(tpy)(bpy)(H_2O)]^{2+}$, and $[Ru(tpy)(bpy)(Cl)]^{+}$. Inorg Chem 48:10720–10725 . doi: 10.1021/ic901477m

20. Österman T, Abrahamsson M, Becker H-C, et al (2012) Influence of Triplet State

Multidimensionality on Excited State Lifetimes of Bis-tridentate Ru^{II} Complexes: A Computational Study. J Phys Chem A 116:1041–1050 . doi: 10.1021/jp207044a

21. Österman T, Persson P (2012) Excited State Potential Energy Surfaces of bistridentate Ru^{II} Complexes – A TD-DFT Study. Chem Phys 407:76–82 . doi: 10.1016/j.chemphys.2012.09.001

22. Breivogel A, Meister M, Förster C, et al (2013) Excited State Tuning of Bis(tridentate) Ruthenium(II) Polypyridine Chromophores by Push-Pull Effects and Bite Angle Optimization: A Comprehensive Experimental and Theoretical Study. Chem - Eur J 19:13745–13760 . doi: 10.1002/chem.201302231

23. Charlot M-F, Pellegrin Y, Quaranta A, et al (2006) A Theoretical Investigation into the Photophysical Properties of Ruthenium Polypyridine-Type Complexes. Chem - Eur J 12:796–812 . doi: 10.1002/chem.200500482

24. Guillemoles J-F, Barone V, Joubert L, Adamo C (2002) A Theoretical Investigation of the Ground and Excited States of Selected Ru and Os Polypyridyl Molecular Dyes. J Phys Chem A 106:11354–11360 . doi: 10.1021/jp021517v

25. Heully J-L, Alary F, Boggio-Pasqua M (2009) Spin-Orbit Effects on the Photophysical Properties of $Ru(bpy)_3^{2+}$. J Chem Phys 131:184308 . doi: 10.1063/1.3254196

26. Nozaki K (2006) Theoretical Studies on Photophysical Properties and Mechanism of Phosphorescence in [fac-Ir (2-phenylpyridine)$_3$]. J Chin Chem Soc 53:101–112

27. Garino C, Terenzi A, Barone G, Salassa L (2016) Teaching Inorganic Photophysics and Photochemistry with Three Ruthenium(II) Polypyridyl Complexes: A Computer-Based Exercise. J Chem Educ 93:292–298 . doi: 10.1021/acs.jchemed.5b00801

28. Arias-Rotondo DM, McCusker JK (2016) The Photophysics of Photoredox Catalysis: a Roadmap for Catalyst Design. Chem Soc Rev 45:5803–5820 . doi: 10.1039/C6CS00526H

29. Neese F (2012) The ORCA Program System. Wiley Interdiscip Rev Comput Mol Sci 2:73–78 . doi: 10.1002/wcms.81

30. Sun Q, Dereka B, Vauthey E, et al (2017) Ultrafast Transient IR Spectroscopy and DFT Calculations of Ruthenium(II) Polypyridyl Complexes. Chem Sci 8:223–230 . doi: 10.1039/C6SC01220E

31. Jonsson H, Mills G, Jacobsen KW (1998) Nudged Elastic Band Method for Finding Minimum Energy Paths of Transitions. In: Berne BJ, Cicotti G, Coker DF (eds) Classical and Quantum Dynamics in Condensed Phase Simulations. World Scientific, pp 385–404

32. Henkelman G, Jóhannesson G, Jónsson H (2000) Methods for Finding Saddle Points and Minimum Energy Paths. In: Schwartz SD (ed) Theoretical Methods in Condensed Phase Chemistry. Kluwer Academic, pp 269–300

33. Göttle AJ, Alary F, Boggio-Pasqua M, et al (2016) Pivotal Role of a Pentacoordinate ^{3}MC State on the Photocleavage Efficiency of a Thioether Ligand in Ruthenium(II) Complexes: A Theoretical Mechanistic Study. Inorg Chem 55:4448–4456 . doi: 10.1021/acs.inorgchem.6b00268

34. Sanz García J, Alary F, Boggio-Pasqua M, et al (2016) Is Photoisomerization Required for NO Photorelease in Ruthenium Nitrosyl Complexes? J Mol Model 22:284 . doi: 10.1007/s00894-016-3138-2

35. Dixon IM, Heully J-L, Alary F, Elliott PIP (2017) Theoretical illumination of highly original photoreactive ^{3}MC states and the mechanism of the photochemistry of Ru(II) tris(bidentate) complexes. Phys Chem Chem Phys 19:27765–27778 . doi: 10.1039/C7CP05532C

36. Harrigan RW, Hager GD, Crosby GA (1973) Evidence for Multiple-State Emission from Ruthenium(II) Complexes. Chem Phys Lett 21:487–490

37. Fleischhauer PD, Adamson AW, Sartori G (1972) Excited States of Metal Complexes and Their Reactions. In: Edwards JO (ed) Progress in Inorganic Chemistry. John Wiley & sons, pp 1–56

38. Damrauer NH, Cerullo G, Yeh A, et al (1997) Femtosecond Dynamics of Excited-State Evolution in $[Ru(bpy)_3]^{2+}$. Science 275:54–57

39. Henry W, Coates CG, Brady C, et al (2008) The Early Picosecond Photophysics of Ru(II) Polypyridyl Complexes: A Tale of Two Timescales. J Phys Chem A 112:4537–4544 . doi: 10.1021/jp711873s

40. Cannizzo A, van Mourik F, Gawelda W, et al (2006) Broadband Femtosecond Fluorescence Spectroscopy of $[Ru(bpy)_3]^{2+}$. Angew Chem Int Ed 45:3174–3176 . doi: 10.1002/anie.200600125

41. Yeh AT, Shank CV, McCusker JK (2000) Ultrafast Electron Localization Dynamics Following Photo-Induced Charge Transfer. Science 289:935–938

42. Hewitt JT, Vallett PJ, Damrauer NH (2012) Dynamics of the ^{3}MLCT in Ru(II) Terpyridyl Complexes Probed by Ultrafast Spectroscopy: Evidence of Excited-State Equilibration and Interligand Electron Transfer. J Phys Chem A 116:11536–11547 . doi: 10.1021/jp308091t

43. Van Houten J, Watts RJ (1976) Temperature Dependence of the Photophysical and Photochemical Properties of the tris(2,2'-bipyridyl) Ruthenium(II) Ion in Aqueous Solution. J Am Chem Soc 98:4853–4858

44. Juris A, Balzani V, Belser P, von Zelewsky A (1981) Characterization of the Excited State Properties of Some New Photosensitizers of the Ruthenium (Polypyridine) Family. Helv Chim Acta 64:2175–2182

45. Amini A, Harriman A, Mayeux A (2004) The Triplet Excited State of Ruthenium(II) bis(2,2′:6′,2″-terpyridine): Comparison between Experiment and Theory. Phys Chem Chem Phys 6:1157–1164 . doi: 10.1039/B313526H

46. Caspar JV, Meyer TJ (1983) Photochemistry of Tris(2,2'-bipyridine) ruthenium(2+) ion ($Ru(bpy)_3^{2+}$). Solvent Effects. J Am Chem Soc 105:5583–5590

47. Schoenlein RW, Chattopadhyay S, Chong HHW, et al (2000) Generation of Femtosecond Pulses of Synchrotron Radiation. Science 287:2237–2240

48. Chen LX, Zhang X (2013) Photochemical Processes Revealed by X-ray Transient Absorption Spectroscopy. J Phys Chem Lett 4:4000–4013 . doi: 10.1021/jz401750g

49. Bressler C, Chergui M (2004) Ultrafast X-ray Absorption Spectroscopy. Chem Rev 104:1781–1812 . doi: 10.1021/cr0206667

50. Bressler C, Chergui M (2010) Molecular Structural Dynamics Probed by Ultrafast X-Ray Absorption Spectroscopy. Annu Rev Phys Chem 61:263–282 . doi: 10.1146/annurev.physchem.012809.103353

51. Saes M, Bressler C, Abela R, et al (2003) Observing Photochemical Transients by Ultrafast X-Ray Absorption Spectroscopy. Phys Rev Lett 90:47403 . doi: 10.1103/PhysRevLett.90.047403

52. Gawelda W, Johnson M, de Groot FMF, et al (2006) Electronic and Molecular Structure of Photoexcited $[Ru^{II}(bpy)_3]^{2+}$ Probed by Picosecond X-ray Absorption Spectroscopy. J Am Chem Soc 128:5001–5009 . doi: 10.1021/ja054932k

53. Sato T, Nozawa S, Tomita A, et al (2012) Coordination and Electronic Structure of Ruthenium(II) tris-2,2′-bipyridine in the Triplet Metal-to-Ligand Charge-Transfer Excited State Observed by Picosecond Time-Resolved Ru K-Edge XAFS. J Phys Chem C 116:14232–14236 . doi: 10.1021/jp3038285

54. Lee C, Yang W, Parr RG (1988) Development of the Colle-Salvetti Correlation-Energy Formula into a Functional of the Electron Density. Phys Rev B 37:785–789

55. Becke AD (1993) A New Mixing of Hartree–Fock and Local Density-Functional Theories. J Chem Phys 98:1372–1377 . doi: 10.1063/1.464304

56. Andrae D, Haeussermann U, Dolg M, et al (1990) Energy-adjusted ab initio Pseudopotentials for the Second and Third Row Transition Elements. Theor Chim Acta 77:123–141

57. Weigend F, Ahlrichs R (2005) Balanced Basis Sets of Split Valence, Triple Zeta Valence and Quadruple Zeta Valence Quality for H to Rn: Design and Assessment of Accuracy. Phys Chem Chem Phys 7:3297–3305 . doi: 10.1039/b508541a

58. Grimme S, Antony J, Ehrlich S, Krieg H (2010) A Consistent and Accurate ab initio Parametrization of Density Functional Dispersion Correction (DFT-D) for the 94 Elements H-Pu. J Chem Phys 132:154104 . doi: 10.1063/1.3382344

59. Grimme S, Ehrlich S, Goerigk L (2011) Effect of the Damping Function in Dispersion Corrected Density Functional Theory. J Comput Chem 32:1456–1465 . doi: 10.1002/jcc.21759

60. Rillema DP, Jones DS (1979) Structure of tris(2,2′-bipyridyl)ruthenium(II) Hexafluorophosphate, $[Ru(bipy)_3][PF_6]_2$; X-ray Crystallographic Determination. J Chem Soc Chem Commun 849–851 . doi: 10.1039/C39790000849

61. Bessel CA, See RF, Jameson DL, et al (1992) Structural Considerations of Terdentate Ligands: Crystal Structures of 2,2′:6′,2″-terpyridine and 2,6-bis(pyrazol-1-yl) pyridine. J Chem Soc Dalton Trans 3223–3228

62. Marenich AV, Cramer CJ, Truhlar DG (2009) Universal Solvation Model Based on Solute Electron Density and on a Continuum Model of the Solvent Defined by the Bulk Dielectric Constant and Atomic Surface Tensions. J Phys Chem B 113:6378–6396 . doi: 10.1021/jp810292n

63. Allouche A-R (2011) Gabedit-A Graphical User Interface for Computational Chemistry Softwares. J Comput Chem 32:174–182 . doi: 10.1002/jcc.21600

64. Ishida H, Tobita S, Hasegawa Y, et al (2010) Recent Advances in Instrumentation for Absolute Emission Quantum Yield Measurements. Coord Chem Rev 254:2449–2458 . doi: 10.1016/j.ccr.2010.04.006

65. Petrenko T, Neese F (2007) Analysis and Prediction of Absorption Band Shapes, Fluorescence Band Shapes, Resonance Raman Intensities, and Excitation Profiles Using the Time-Dependent Theory of Electronic Spectroscopy. J Chem Phys 127:164319 . doi: 10.1063/1.2770706

66. Petrenko T, Neese F (2012) Efficient and Automatic Calculation of Optical Band Shapes and Resonance Raman Spectra for Larger Molecules within the Independent Mode Displaced Harmonic Oscillator Model. J Chem Phys 137:234107 . doi: 10.1063/1.4771959

67. Bradley PG, Kress N, Hornberger BA, et al (1981) Vibrational Spectroscopy of the Electronically Excited State. 5. Time-Resolved Resonance Raman Study of Tris(bipyridine)ruthenium(II) and Related Complexes. Definitive Evidence for the "Localized" MLCT State. J Am Chem Soc 103:7441–7446

68. Herbol HC, Stevenson J, Clancy P (2017) Computational Implementation of Nudged Elastic Band, Rigid Rotation, and Corresponding Force Optimization. J Chem Theory Comput 13:3250–3259 . doi: 10.1021/acs.jctc.7b00360

69. Smidstrup S, Pedersen A, Stokbro K, Jónsson H (2014) Improved Initial Guess for Minimum Energy Path Calculations. J Chem Phys 140:214106

70. Chen P, Meyer TJ (1998) Medium Effects on Charge Transfer in Metal Complexes. Chem Rev 98:1439–1478

71. Thompson DW, Fleming CN, Myron BD, Meyer TJ (2007) Rigid Medium Stabilization of Metal-to-Ligand Charge Transfer Excited States. J Phys Chem B 111:6930–6941 . doi: 10.1021/jp068682l

72. Klamt A, Schüürmann G (1993) COSMO: a New Approach to Dielectric Screening in Solvents with Explicit Expressions for the Screening Energy and its Gradient. J Chem Soc Perkin Trans 2 799–805

73. Ito A, Meyer TJ (2012) The Golden Rule. Application for Fun and Profit in Electron Transfer, Energy Transfer, and Excited-State Decay. Phys Chem Chem Phys 14:13731–13745 . doi: 10.1039/c2cp41658a

74. Wrighton M, Morse DL (1974) The Nature of the Lowest Excited State in Tricarbonylchloro-1,10-phenanthrolinerhenium(I) and Related Complexes. J Am Chem Soc 96:998–1003

75. Liotard D, Penot J-P (1981) Critical Paths and Passes: Application to Quantum Chemistry. In: Della Dora J, Demongeot J, Lacolle B (eds) Numerical methods in the study of critical phenomena. Springer, pp 213–221

76. Liotard DA (1992) Algorithmic Tools in the Study of Semiempirical Potential Surfaces. Int J Quantum Chem 44:723–741

77. Fukui K (1981) The Path of Chemical Reactions-the IRC Approach. Acc Chem Res 14:363–368

78. Sun Q, Mosquera-Vazquez S, Lawson Daku LM, et al (2013) Experimental Evidence of Ultrafast Quenching of the ^{3}MLCT Luminescence in Ruthenium(II) Tris-bipyridyl Complexes via a ^{3}dd State. J Am Chem Soc 135:13660–13663 . doi: 10.1021/ja407225t

79. Mukuta T, Fukazawa N, Murata K, et al (2014) Infrared Vibrational Spectroscopy of $[Ru(bpy)_2(bpm)]^{2+}$ and $[Ru(bpy)_3]^{2+}$ in the Excited Triplet State. Inorg Chem 53:2481–2490 . doi: 10.1021/ic402474t

80. Sanz García J, Alary F, Boggio-Pasqua M, et al (2015) Establishing the Two-Photon Linkage Isomerization Mechanism in the Nitrosyl Complex *trans*-$[RuCl(NO)(py)_4]^{2+}$ by DFT and TDDFT. Inorg Chem 54:8310–8318 . doi: 10.1021/acs.inorgchem.5b00998

81. Shaik S, Danovich D, Fiedler A, et al (1995) Two-State Reactivity in Organometallic Gas-Phase Ion Chemistry. Helv Chim Acta 78:1393–1407

82. Schröder D, Shaik S, Schwarz H (2000) Two-State Reactivity as a New Concept in Organometallic Chemistry. Acc Chem Res 33:139–145 . doi: 10.1021/ar990028j

83. Marian CM (2012) Spin-orbit Coupling and Intersystem Crossing in Molecules. Wiley Interdiscip Rev Comput Mol Sci 2:187–203 . doi: 10.1002/wcms.83

84. Harvey JN, Aschi M, Schwarz H, Koch W (1998) The Singlet and Triplet States of Phenyl Cation. A Hybrid Approach for Locating Minimum Energy Crossing Points between Non-Interacting Potential Energy Surfaces. Theor Chem Acc 99:95–99

85. Poli R, Harvey JN (2003) Spin Forbidden Chemical Reactions of Transition Metal Compounds. New Ideas and New Computational Challenges. Chem Soc Rev 32:1–8 . doi: 10.1039/b200675h

86. Harvey JN, Poli R, Smith KM (2003) Understanding the Reactivity of Transition Metal Complexes Involving Multiple Spin States. Coord Chem Rev 238:347–361

87. Harvey JN (2014) Spin-Forbidden Reactions: Computational Insight into Mechanisms and Kinetics: Spin-Forbidden Reactions. Wiley Interdiscip Rev Comput Mol Sci 4:1–14 . doi: 10.1002/wcms.1154

88. Kreitner C, Heinze K (2016) Excited State Decay of Cyclometalated Polypyridine Ruthenium Complexes: Insight from Theory and Experiment. Dalton Trans 45:13631–13647 . doi: 10.1039/C6DT01989G

89. Englman R, Jortner J (1970) The Energy Gap Law for Radiationless Transitions in Large Molecules. Mol Phys 18:145–164

90. Teller E (1937) The Crossing of Potential Surfaces. J Phys Chem 41:109–116

TOC graphic

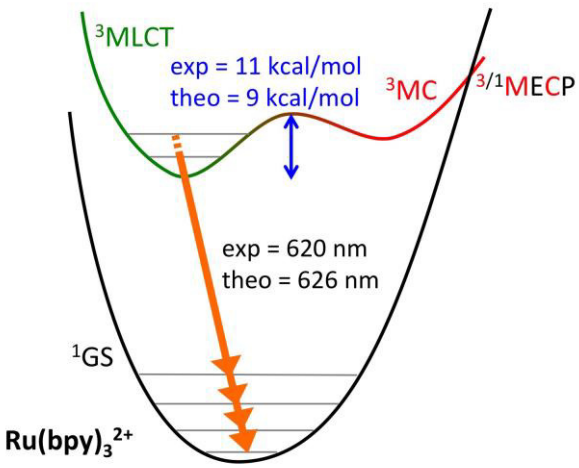
^{3}MLCT
exp = 11 kcal/mol
theo = 9 kcal/mol
^{3}MC
$^{3/1}$MECP
exp = 620 nm
theo = 626 nm
^{1}GS
Ru(bpy)$_3^{2+}$